Mechanistic and Metabolic Inferences from the Binding of Substrate Analogues and Products to Arginase[†,‡]

J. David Cox,[§] Evis Cama,[§] Diana M. Colleluori,[||] Stephanie Pethe,[⊥] Jean-Luc Boucher,[⊥] Daniel Mansuy,[⊥] David E. Ash,[||] and David W. Christianson*[,§]

Roy and Diana Vagelos Laboratories, Department of Chemistry, University of Pennsylvania, Philadelphia, Pennsylvania 19104-6323, Department of Biochemistry, Temple University School of Medicine, Philadelphia, Pennsylvania 19140, and UMR 8601, Université Paris V, 45 rue des Saints-Pères, 75270 Paris Cedex 06, France

Received October 3, 2000; Revised Manuscript Received December 21, 2000

ABSTRACT: Arginase is a binuclear Mn^{2+} metalloenzyme that catalyzes the hydrolysis of L-arginine to L-ornithine and urea. X-ray crystal structures of arginase complexed to substrate analogues N^{ω}-hydroxy-L-arginine and N^{ω}-hydroxy-*nor*-L-arginine, as well as the products L-ornithine and urea, complete a set of structural "snapshots" along the reaction coordinate of arginase catalysis when interpreted along with the X-ray crystal structure of the arginase-transition-state analogue complex described in Kim et al. [Kim, N. N., Cox, J. D., Baggio, R. F., Emig, F. A., Mistry, S., Harper, S. L., Speicher, D. W., Morris, Jr., S. M., Ash, D. E., Traish, A. M., and Christianson, D. W. (2001) *Biochemistry 40*, 2678−2688]. Taken together, these structures render important insight on the structural determinants of tight binding inhibitors. Furthermore, we demonstrate for the first time the structural mechanistic link between arginase and NO synthase through their respective complexes with N^{ω}-hydroxy-L-arginine. That N^{ω}-hydroxy-L-arginine is a catalytic intermediate for NO synthase and an inhibitor of arginase reflects the reciprocal metabolic relationship between these two critical enzymes of L-arginine catabolism.

Arginase, a 105 kDa homotrimer containing a binuclear manganese cluster in each protomer, catalyzes the hydrolysis of L-arginine to form L-ornithine and urea through a metal-activated hydroxide mechanism (*1*−*4*). Enzyme activity is found at highest levels in mammalian liver (*5*), where this reaction constitutes the final cytosolic step of the urea cycle. The flux of substrate through this step is considerable, since the average adult excretes about 10 kg of urea/year. In addition to liver, arginase activity is detected in several nonhepatic tissues lacking a complete urea cycle, such as gastrointestinal smooth muscle (*6*), penile corpus cavernosum smooth muscle (*7*), and activated macrophages (*8*−*16*). In these tissues, activity is believed to result primarily from a second isozyme (arginase II) (*17*) that is distinct in immunologic properties, amino acid sequence, and subcellular location from the more abundant liver isozyme (arginase I).

Arginase II probably plays a more important role in regulating NO biosynthesis by attenuating the levels of L-arginine available to NO synthase (Figure 1). The regulatory relationship between arginase and NO synthase is reciprocal to some degree, since the stable intermediate in NO biosynthesis, N^{ω}-hydroxy-L-arginine (NOHA)[1] (*18*−*22*), is a modest competitive inhibitor of arginase with $K_i = 10-42\ \mu M$ (Figure 1, Table 1) (*9*, *23*). Sufficient concentrations of NOHA are produced in endothelial cells and activated macrophages to inhibit arginase (*24*−*25*). NOHA binds to NO synthase with $K_M = 7-59\ \mu M$ (*18*, *19*, *26*−*29*) in a deep active-site channel between the heme and surrounding hydrophobic residues (*30*−*32*). The hydroxyguanidinium moiety of NOHA packs against the heme group in the enzyme active site, but does not coordinate to the heme iron or hydrogen bond with any porphyrin ring atoms (*30*, *31*). On the basis of the inhibitory properties of NOHA against arginase (*9*, *23*), a number of *N*-hydroxy analogues have been synthesized and evaluated as arginase inhibitors (*23*, *33*, *34*). The most potent of these compounds is N^{ω}-hydroxy-*nor*-L-arginine (*nor*-NOHA; $K_i = 0.5\ \mu M$) (Table 1) (*23*), which upon binding arginase, is proposed to either displace the metal-bridging hydroxide ion or form a hydrogen bond with it (*23*).

The 2.1 Å resolution crystal structure of trimeric rat liver arginase reveals that the overall fold of the arginase monomer

[†] Supported by National Institute of Health Grants GM49758 (D.W.C.) and DK44841 (D.E.A.).

[‡] Atomic coordinates of arginase complexes have been deposited in the Research Collaboratory for Structural Bioinformatics with the following accession codes: complex with N^{ω}-hydroxy-L-arginine, 1HQF; complex with L-ornithine and urea, 1HQG; complex with N^{ω}-hydroxyl-*nor*-L-arginine, 1HQH.

* To whom correspondence should be addressed. E-mail: chris@xtal.chem.upenn.edu. Phone: (215) 898-5714. Fax: (215) 573-2201.

[§] University of Pennsylvania.

[||] Temple University School of Medicine.

[⊥] Université Paris V.

[1] Abbreviations: ABH, (*S*)-2-amino-6-boronohexanoic acid; BEC, *S*-(2-boronoethyl)-L-cysteine; CHES, 2-(*N*-cyclohexylamino)-ethanesulfonic acid; CSD, Cambridge Structural Database; EDTA, ethylenediamine tetraacetic acid; HEPES, *N*-(2-hydroxyethyl)-piperazine-*N*-2-ethanesulfonic acid; IPTG, isopropyl-β-D-thiogalactopyranoside; LB, Luria-Bertani; NO, nitric oxide; NOHA, N^{ω}-hydroxy-L-arginine; *nor*-NOHA, N^{ω}-hydroxy-*nor*-L-arginine; PCR, polymerase chain reaction; PMSF, phenylmethanesulfonyl fluoride; SDS−PAGE, sodium dodecyl sulfate−polyacrylamide gel electrophoresis.

10.1021/bi002318+ CCC: $20.00
Published on Web 02/02/2001

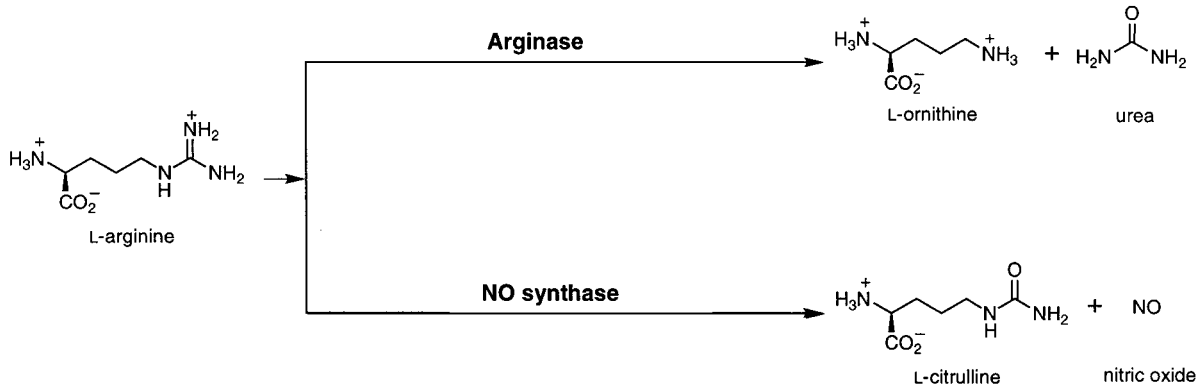

FIGURE 1: Reciprocal coordination of arginase and nitric oxide pathways; note that N^{ω}-hydroxy-L-arginine is an intermediate in the NO synthase reaction.

Table 1: Inhibition of Arginase by NOHA, *nor*-NOHA, and Their Analogues

Compound		IC_{50} (μM)[a]	K_i (μM)
NOHA	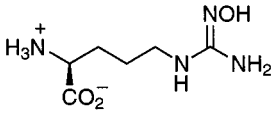	20 ± 2	10-42[b]
descarboxy-NOHA	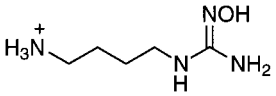	1000 ± 400	
nor-NOHA	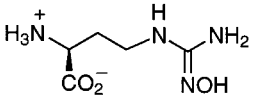	1 ± 0.5	0.5[c]
descarboxy-*nor*-NOHA	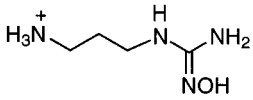	300 ± 50	
des-(α-amino)-*nor*-NOHA	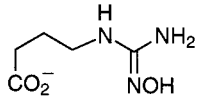	5000 ± 1000	

[a] Mean values ± standard deviation from four experiments. [b] Refs *9* and *23*. [c] Ref *23*.

belongs to the α/*β* family, consisting of a parallel, eight-stranded *β*-sheet flanked on both sides by numerous α-helices (*35*). Analysis of the crystal structure indicates that L-arginine hydrolysis proceeds via nucleophilic attack by a metal-activated solvent molecule symmetrically bridging the two Mn^{2+} ions (Mn^{2+}_A−Mn^{2+}_B separation = 3.3 Å) (*35*). This binuclear manganese cluster is located at the bottom of a ~15 Å-deep active-site cleft in each monomer (*35*). The more deeply situated metal is designated Mn^{2+}_A. Hydroxide ion symmetrically bridges Mn^{2+}_A and Mn^{2+}_B and donates a hydrogen bond to Oδ1 of Asp-128; Oδ2 of Asp-128 coordinates to Mn^{2+}_A. These interactions orient the remaining lone electron pair of metal-bridging hydroxide for nucleophilic attack on the substrate, L-arginine, which is postulated to form a salt link with Glu-277 (*35*). Nucleophilic attack yields a tetrahedral intermediate that collapses to yield the products L-ornithine and urea. 2(*S*)-Amino-6-boronohexanoic acid (ABH; K_d = 0.11 μM) (*36*, *37*) and *S*-(2-boronoethyl)-L-cysteine (BEC; K_d = 2.22 μM) (*38*) bind to arginase as the hydrated tetrahedral boronate anions, revealing active-site interactions expected for the tetrahedral intermediate and its flanking transition states (*7*, *36*−*38*).

To provide additional "snapshots" of structures along the reaction coordinate of arginase catalysis and to probe structural aspects of the reciprocal metabolic relationship between arginase and NO synthase outlined in Figure 1, we have determined the X-ray crystal structures of arginase complexed with the substrate analogues NOHA and *nor*-NOHA, as well as the products L-ornithine (K_i = 1.0 mM) and urea (K_i = 880 mM) (*39*−*41*). These structures highlight new details in the reaction coordinate of arginase catalysis and they render important insights on the structural determinants of tight binding inhibitors. Furthermore, we outline the structural and chemical link between arginase and NO synthase with the different molecular recognition strategies for NOHA binding.

MATERIALS AND METHODS

Enzyme Preparation. Nucleotide primers were purchased from Ransom Hill Bioscience, Inc. DNA sequencing was provided by the University of Pennsylvania DNA Sequencing facility. Restriction enzymes were purchased from New England Biolabs. L-[guanido-^{14}C]Arginine (specific activity 2.5 GBq mmol^{-1}) was purchased from NEN Life Science Products. All other reagents were of the highest purity commercially available.

Recombinant wild-type arginase was prepared as described by Cavalli and colleagues (*42*). For the first PCR reaction, site-directed mutagenesis was carried out by the method of Higuchi and colleagues (*43*), with modifications as described by Cavalli and colleagues (*42*). His-141 was mutated to cysteine using the oligonucleotides 5′-GGGAATCTG**TGC**-GGGCAACCGG-3′ and 5′-CCGGTTGCCC**GCA**CAGAT-TCCC-3′ as the forward and reverse primers, respectively. For the first primary PCR reaction, the pARG−*Pst*I primer was used with the appropriate sense mutagenic oligonucleotide primer (*42*). For the second primary PCR reaction, the following primer was paired with the appropriate antisense mutagenic oligonucleotide primer: 5′-**GAATTC**ATATGA-GCTCCAAGCCAAAG-3′, designated pARG-NdeI/EcoR1, with the *Nde*I site underlined and the *Eco*R1 site in bold. The secondary PCR was carried out using pARG-*Nde*I/*Eco*R1 and pARG−*Pst*I as primers and the two PCR fragments from the primary reaction as templates. The resulting full-length mutated cDNA was digested with *Eco*R1 and *Pst*I and ligated into *Eco*R1 and *Pst*I-digested pBLUE-SCRIPT, followed by transformation into *E. coli* DH5α. The DNA from positive colonies was sequenced to confirm the desired mutation and to ensure the absence of unwanted mutations.

The pBLUESCRIPT vector carrying the arginase cDNA and the pET29b vector (Novagen) were digested with *Nde*I and *Bam*H1, and the DNA was separated by 1% agarose gel. The linear pET29b vector and the 1-kb arginase cDNA were extracted from the gel (Qiagen QIAquick Gel Extraction Kit), ligated, and transformed into *E. coli* BL21(DE3) for expression. The DNA from a positive clone was purified and sequenced. Each positive clone was grown overnight with shaking at 37 °C in LB containing 30 μg/mL kanamycin. From this culture, 15% glycerol stocks were prepared and frozen at −70 °C. The frozen stocks were the source of cells for subsequent expression of protein.

An aliquot of the frozen cell stock was streaked onto LB plates containing 30 μg/mL Kanamycin and incubated overnight at 37 °C. Cells from this plate were used to inoculate 6 L of LB media containing 30 μg/mL kanamycin. This culture was grown at 37 °C with shaking to an A_{600} of 0.8 and then induced with 0.2 mg/mL IPTG. After 3 h, the cells were harvested by centrifugation at 5000*g* for 30 min. The cell pellet was stored frozen at −70 °C overnight. The cells were thawed and resuspended in 1 mM PMSF, 10 mM EDTA, and 50 mM HEPES−KOH (pH 7.5). The H141C arginase was purified from the lysed cells by a modification of the method described by Cavalli and colleagues (*42*). Specifically, partially purified protein samples were subject to chromatography on a Sigma-Red 120 dye ligand column, instead of the Amicon-Green dye ligand column described previously, and eluted with a linear gradient of 0.0−0.3 M KCl in 50 mM HEPES−KOH (pH 7.5). Protein purity was determined to be >95% by SDS−PAGE analysis under reducing conditions.

H141C arginase was assayed as described by Cavalli and colleagues (*42*), with the following modifications. Assays were performed in 100 mM CHES−KOH (pH 9) containing 100 μM $MnCl_2$. L-Arginine concentrations were varied from 0.5 to 20 mM. Upon addition of the enzyme to the reaction mixture (final concentration of 1.5−15 μg/mL), the reaction was allowed to proceed for 60 min. The data were analyzed using double-reciprocal plots of initial velocity measurements.

Synthesis and Inhibitory Properties of NOHA, nor-NOHA, and Their Analogues. The NOHA samples were purchased from Alexis Biochemicals (San Diego) and L-arginine from Sigma. The *nor*-NOHA samples were synthesized as previously described (*44*). The synthesis of descarboxy-NOHA, descarboxy-*nor*-NOHA, and des-(α-amino)-*nor*-NOHA will be published elsewhere. Structures were established by ^{1}H and ^{13}C NMR spectroscopy. The IC_{50} values of these compounds toward purified rat liver arginase were determined as reported previously (*33*).

Crystallography. Wild-type and H141C arginases were crystallized using the hanging drop vapor diffusion method as described previously (*45*). Briefly, 5 μL drops of precipitant buffer containing 50 mM bicine (pH 8.5 at room temperature), 12−18% PEG 8000, and 5 mM $MnCl_2$ were added to 5 μL drops containing approximately 12−16 mg/mL protein on a silanized cover slip at 4 °C. The cover slip was sealed over a reservoir containing 1 mL of the precipitant buffer. Pyramidal crystals with approximate dimensions 0.3 × 0.3 × 0.3 mm^3 appeared after four weeks and were nearly isomorphous with those of wild-type arginase (*45*); crystals belonged to space group $P3_2$ with unit cell parameters listed in Table 2. Crystals of the wild-type arginase−NOHA complex and the H141C arginase−L-ornithine−urea ternary complex were prepared by soaking crystals for at least 6 days in 18% PEG 8000, 50 mM bicine (pH 8.5 at room temperature), 5 mM $MnCl_2$, and 5 mM of either NOHA or L-arginine; the buffer was refreshed once a day. Catalytic turnover of H141C arginase in the crystal yielded L-ornithine and urea from the substrate L-arginine contained in the crystal soaking buffer. Due to the instability of *nor*-NOHA at pH >8.0, crystals of wild-type arginase were first equilibrated for 2 days in a stabilizing buffer solution of 18% PEG 8000, 50 mM HEPES (pH 7.5 at room temperature), and 5 mM $MnCl_2$, and then transferred to an identical buffer solution containing 5 mM *nor*-NOHA for 6 days (the buffer was refreshed once a day).

Prior to data collection, crystals were gradually transferred to a cryoprotectant solution containing 30% glycerol in addition to the original precipitant solution and flash-cooled with liquid nitrogen. All X-ray diffraction data, with the exception of those collected from crystals of the arginase−*nor*-NOHA complex, were collected on a Mar 345 mm image plate detector at Stanford Synchrotron Radiation Laboratory beamline 7-1 (λ = 1.08 Å) at the Stanford Linear Accelerator Center in Menlo Park, CA. Intensity data for the arginase−*nor*-NOHA complex were collected on a Mar 165 mm single element CCD detector at the Advanced Photon Light Source beamline 17-ID (λ = 1.00 Å) at the Argonne National Laboratory (Argonne, IL). Intensity data integration and

Table 2: Data Collection and Refinement Statistics for Arginase-Ligand Complexes

arginase ligand(s)	N^{ω}-hydroxy-L-arginine	N^{ω}-hydroxy-*nor*-L-arginine	L-ornithine + urea
unit cell parameters (Å)	$a = b = 88.0$ $c = 112.0$	$a = b = 88.0$ $c = 112.4$	$a = b = 88.2$ $c = 106.5$
no. of crystals	2	1	1
no. of measured reflections	31 263	55 538	111 757
no. of unique reflections	17 524	22 632	59 154
resolution range (Å)	30.0−2.9	25.0−2.8	30.0−2.0
completeness of data overall (last shell) (%)	83.7 (86.7)	98.9 (100.0)	94.3 (96.9)
R_{sym} overall (last shell)[a]	0.064 (0.302)	0.045 (0.319)	0.061 (0.350)
no. of reflections used in refinement (in test set)	16 344 (781)	22 623 (1074)	56 392 (2841)
R_{cryst} (R_{free})[b]	0.265 (0.289)	0.259 (0.286)	0.232 (0.243)
no. of water molecules in final cycle of refinement	5	8	57
rms deviation from ideal bond lengths (Å)	0.008	0.008	0.005
rms deviation from ideal bond angles (deg)	1.5	1.5	1.3
rms deviation from ideal dihedral angles (deg)	23.4	23.2	22.6
rms deviation from ideal improper dihedral angles (deg)	1.1	1.1	0.8
RCSB accession codes	1HQF	1HQH	1HQG

[a] R_{sym} for replicate reflections, $R = \sum|I_h - \langle I_h\rangle|/\sum\langle I_h\rangle$; I_h = intensity measured for reflection h; $\langle I_h\rangle$ = average intensity for reflection h calculated from replicate data. [b] Crystallographic R factor, $R_{cryst} = \sum||F_o| - |F_c||/\sum|F_o|$ for reflections contained in the working set. Free R factor, $R_{free} = \sum||F_o| - |F_c||/\sum|F_o|$ for reflections contained in the test set held aside during refinement (5% of total). $|F_o|$ and $|F_c|$ are the observed and calculated structure factor amplitudes, respectively.

reduction were performed using the HKL suite of programs (*46*).

Initial phasing was achieved by molecular replacement using AMoRe (*47*, *48*); the structure of the native arginase trimer less the atoms of the variant side chain (for H141C) and all water molecules was used as a search probe, which yielded unique and unambiguous solutions for each structure. All structures were refined using torsion angle molecular dynamics ($T_{initial} = 5000$ K) with energy minimization, using the maximum likelihood algorithm as implemented in CNS (*49*). Strict noncrystallographic symmetry constraints were initially employed in refinement, and these were relaxed to appropriately weighted restraints as judged by R_{free} as refinement progressed. After initial rounds of refinement, electron density for the ligands and the variant C141 side chain was clear and unambiguous in electron density maps generated with Fourier coefficients $2|F_o| - |F_c|$ and $|F_o| - |F_c|$ and phases calculated from the in-progress atomic model. A continuous electron density peak adjacent to the variant C141 side chain was modeled as a disulfide-linked β-mercaptoethanol molecule. Iterative rounds of refinement and rebuilding were performed with CNS and O, respectively (*49*, *50*). Individual B factors were refined and a bulk solvent correction was applied. Refinement ultimately converged to final crystallographic R-factors of 0.232−0.265 (R_{free}: 0.243−0.289) and excellent stereochemistry. Data collection and refinement statistics are reported in Table 2. Figures were generated using BOBSCRIPT and Raster3D (*51*, *52*).

Cambridge Structural Database Analysis. To assist in the interpretation of the electron density map of the arginase−L-ornithine−urea ternary complex, we extracted and analyzed the stereochemistry of urea−metal coordination interactions in the Cambridge Structural Database (CSD) (*53*). The CSD was installed on a Dell computer and coordinate entries were searched using the program ConQuest. The initial search targeted a urea molecule with either an oxygen or nitrogen atom within 1.9−3.0 Å of any metal ion, excluding actinides and lanthanides. After the elimination of structures with crystallographic R-factors greater than 0.10 or other explicitly defined errors, a total of 45 coordinate entries remained. Of these, 41 entries yielded 93 unique and independent urea oxygen−metal coordination interactions; four entries yielded five unique and independent urea nitrogen−metal coordination interactions. Microsoft Excel was used to determine the average lengths and angles of retrieved coordination interactions. Scatterplots were generated by superimposing the urea molecules of each retrieval and allowing the coordinated metal ions to fall into their positions relative to the reference urea molecule. This procedure was performed on a Silicon Graphics terminal using the program O (*50*).

RESULTS

H141C Arginase−L-Ornithine−Urea Ternary Complex. Activity assays of H141C arginase yield K_M and k_{cat} values of 3.0 mM and 0.3 s^{-1}, respectively, indicating 0.06% of wild-type activity (for the wild-type enzyme, $K_M = 1.4$ mM and $k_{cat} = 250$ s^{-1}) (*42*). Initially, we hypothesized that we might trap an intact enzyme−substrate complex using crystalline H141C arginase due to the significant activity loss of this variant. However, on the time-scale of the X-ray crystallographic experiment, H141C arginase is sufficiently active that incubation of the crystalline enzyme with substrate L-arginine exclusively yields the bound products L-ornithine and urea.

The binding of products L-ornithine and urea to arginase does not trigger any significant tertiary or quaternary structural changes, and the rms deviation of 314 Cα atoms is 0.3 Å between native arginase and the H141C arginase−products complex. The average thermal B factors of the protein, ornithine, and urea are 26, 49, and 62 $Å^2$, respec-

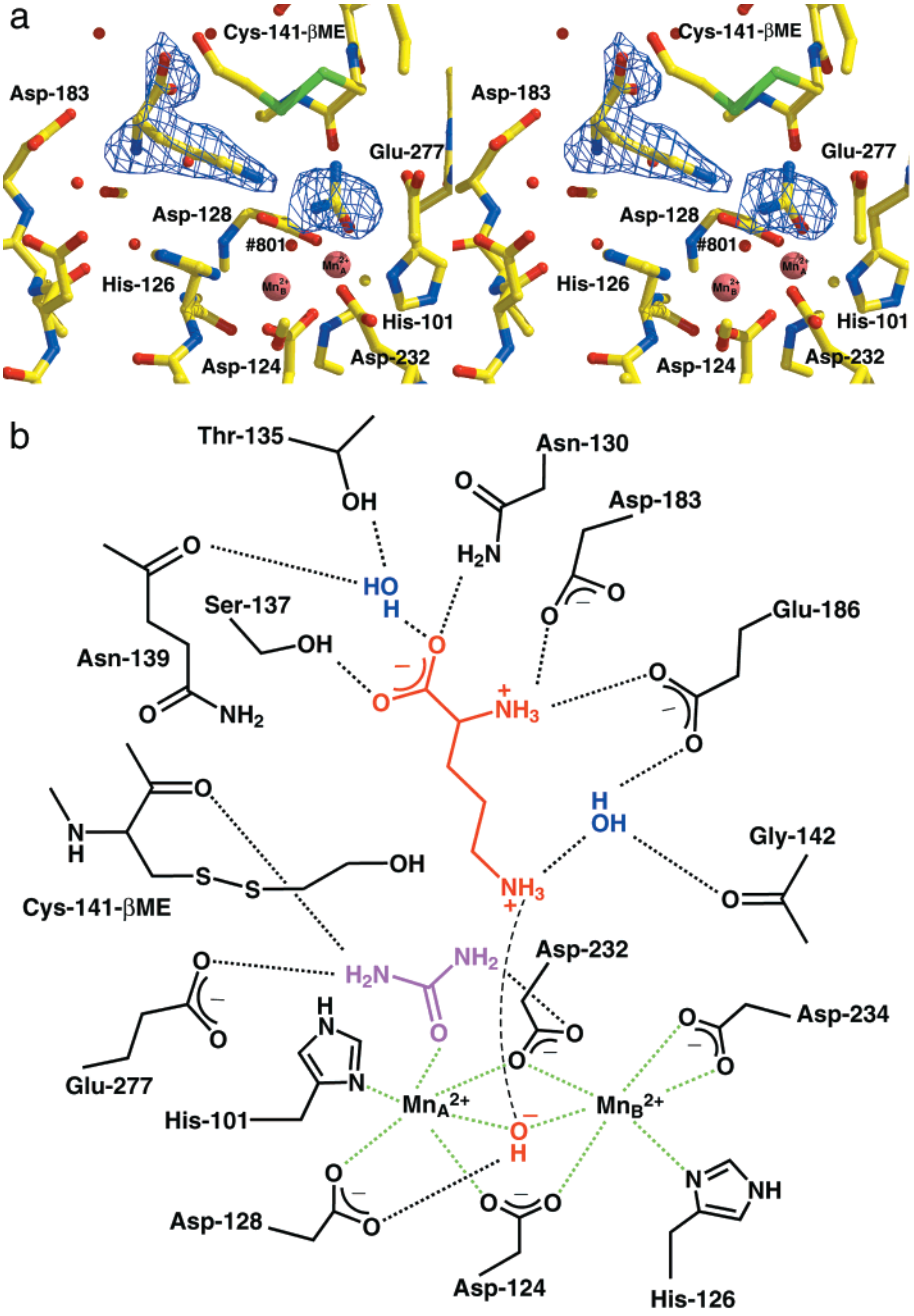

FIGURE 2: H141C Arginase−L-ornithine−urea ternary complex. (a) Omit electron density map of L-ornithine and urea in the arginase active site calculated with SIGMAA-weighted (*79*) coefficients $|F_o| - |F_c|$ averaged over the three monomers in the asymmetric unit. The map is contoured at 3.5σ and selected active-site residues are indicated. Atoms are color-coded as follows: C = yellow, O = red, N = blue, S = green; water molecules appear as red spheres. The side chain of Cys-141 forms a disulfide linkage with a molecule of β-mercaptoethanol. (b) Summary of intermolecular interactions. Manganese coordination interactions are designated by green dashed lines, and hydrogen bonds are indicated by black dashed lines.

tively. The omit map in Figure 2a reveals clear and unambiguous density for L-ornithine. The ϵ-NH_3^+ group of L-ornithine donates a hydrogen bond to the metal bridging hydroxide ion (Nϵ···O separation = 2.7 Å). Additionally, this amino nitrogen is within 2.8 Å of both nitrogen atoms of urea; however, this must reflect a van der Waals interaction and not a hydrogen bond interaction, since the urea nitrogen lone electron pairs are delocalized in the ureido π system and are not available for hydrogen bonding. The ϵ-NH_3^+ group of L-ornithine is 2.7 Å from the sulfur atom of β-mercaptoethanol that is disulfide-linked to the Cys-141 side chain. Although an unreasonably close contact of 1.4 Å is observed between the carboxylate of L-ornithine and the hydroxyl group of the Cys-141-linked β-mercaptoethanol molecule, it is likely that the Cys-141 modification and L-ornithine binding are mutually exclusive. Since the average thermal *B* factors for L-ornithine and Cys-141-β-mercaptoethanol (both 49 Å^2) are higher than that of the protein (26 Å^2), this may reflect compensation for diminished occupancy during temperature factor refinement.

The α-carboxylate and α-amino groups of L-ornithine make numerous direct and water-mediated hydrogen bonds with numerous conserved residues in the arginase active site (Figure 2b). Carboxylate oxygen O1 accepts a hydrogen bond from the hydroxyl oxygen of Ser-137; carboxylate oxygen O2 accepts a hydrogen bond from Asn-130 (O···Nδ separa-

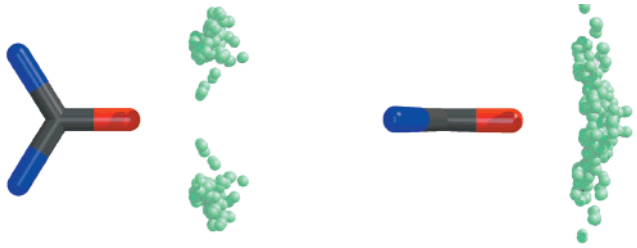

FIGURE 3: Scatterplot showing two perpendicular orientations of urea C═O···metal interactions (C_{2v} symmetry equivalents are indicated). The urea oxygen is red, nitrogens are blue, and the aquamarine spheres represent metal ions. For the 93 interactions retrieved from the CSD, the average distance is 2.0 Å and the average angle is 135°; short, strong interactions tend to cluster at smaller C═O···metal angles, indicative of an interaction with the sp^2-lone electron pairs of the urea carbonyl oxygen.

tion = 2.9 Å) and is within hydrogen-bonding distance to two water molecules, 842 and 843, with O···O separations of 2.8 and 3.0 Å, respectively. Water 842 in turn hydrogen bonds to the side-chain hydroxyl of Thr-135 (2.8 Å) and the backbone carbonyl of Asn-139 (2.7 Å). Water 843 also hydrogen bonds to the α-amino group of L-ornithine (2.6 Å), Oε2 of Glu-186 (2.7 Å), and the backbone carbonyl of Gly-142 (2.8 Å). The α-amino group of L-ornithine donates hydrogen bonds to Oδ2 of Asp-183 and Oε1 of Glu-186.

The product urea molecule is also visible in the omit map, although one urea nitrogen atom is not entirely well-defined by electron density (Figure 2a). Nevertheless, this electron density is consistent with coordination of the urea carbonyl oxygen to Mn^{2+}_A (O···Mn separation = 2.0 Å). This changes the coordination geometry of Mn^{2+}_A from square pyramidal in native arginase (*35*) to distorted octahedral (Mn^{2+}_B coordination remains unchanged as distorted octahedral). The ureido NH_2 groups contact several active-site residues. Urea nitrogen N1 is within 3.2 Å of Asp-232, the metal-bridging solvent molecule, and the ε-NH_3^+ group of L-ornithine. Urea nitrogen N2 is within 3.2 Å of the backbone carbonyl oxygen of Cys-141, Glu-277, Sδ of Cys-141-β-mercaptoethanol, and the ε-NH_3^+ group of L-ornithine. Importantly, the hydrogen bond observed between urea nitrogen N2 and Oε2 of Glu-277 is reminiscent of the proposal that Glu-277 salt links with the substrate, L-arginine, prior to catalysis (*35*). Here, Glu-277 is now implicated in product binding as well.

Given the moderate quality of the urea peak in the electron density map of Figure 2a, we used the results of our CSD analysis to strengthen our interpretation of the urea binding mode in the arginase active site. Since our analysis of the CSD yields 93 unique and independent urea oxygen−metal coordination interactions, but only five unique and independent urea nitrogen−metal coordination interactions, we conclude that urea preferentially coordinates to a metal ion through its carbonyl oxygen atom. Our interpretation of urea binding to arginase reflects this preference. The statistics calculated from the CSD retrievals indicate that for the group of 93 urea oxygen−metal interactions, the average urea C═O···metal separation is 2.06 ± 0.11 Å and the average C═O···metal angle is 134.2 ± 5.4°; for a subgroup of five interactions occurring specifically with manganese, the average urea C═O···metal separation is 2.14 ± 0.09 Å and the average C═O···metal angle is 134.6 ± 1.9°. The scatterplot of Figure 3 reveals that metal ions tend to cluster around the sp^2-lone electron pairs of the urea carbonyl oxygen. In the arginase−L-ornithine−urea complex, the urea C═O···Mn^{2+}_A separation and angle are 1.8 Å and 141.5°, respectively, consistent with the parameters obtained from the CSD analysis. Since the complex was refined without restraining urea C═O···Mn^{2+}_A interactions, that refinement converged to parameters consistent with those derived from the CSD analysis strengthens our interpretation of the urea electron density peak.

Parenthetically, we note that for the five urea nitrogen-metal coordination interactions retrieved from the CSD, the average urea N···metal separation is 2.36 ± 0.04 Å and the average C−N···metal angle is 113.5 ± 2.3°. In each of the five structures, the urea nitrogen is pyramidalized such that metal coordination is achieved by a nitrogen sp^3 lone electron pair. Notably, these structures involve only Ag^+ and Co^{2+} interactions and the urea molecules form novel polymer sheets in the crystal lattice. Possibly, this unusual aspect of the crystal lattice plays a role in directing the less-favorable urea N···metal coordination interaction.

Intriguingly, a metal-bridging hydroxide ion is also observed in the arginase−L-ornithine−urea ternary complex, and it symmetrically bridges the binuclear manganese cluster with O···Mn^{2+} separations of 2.1 Å. The Mn^{2+}_A−Mn^{2+}_B separation is 3.3 Å, which is identical to that found in the native enzyme (*35*). On the basis of this structure, we now clarify an additional feature of the catalytic mechanism of arginase: the release of products L-ornithine and urea can occur *after* the binding of the water molecule that regenerates the catalytic nucleophile, metal-bridging hydroxide.

Wild-Type Arginase−NOHA Complex. The binding of NOHA does not trigger any major tertiary or quaternary structural changes, and the rms deviation of 314 Cα atoms is 0.37 Å between native arginase and the arginase−NOHA complex. The average thermal B factors of the protein and NOHA are 85 and 60 $Å^2$, respectively. The omit map of Figure 4a reveals that the hydroxyl oxygen of NOHA displaces the metal-bridging hydroxide ion of the native enzyme and asymmetrically bridges the binuclear Mn^{2+} cluster with O···Mn^{2+}_A and O···Mn^{2+}_B separations of 2.6 and 2.2 Å, respectively. Importantly, Daghigh and colleagues first predicted that the hydroxyl group of NOHA would displace metal-bound hydroxide (*9*). Additionally, this is in agreement with subsequent electron paramagnetic resonance studies of the arginase−NOHA complex showing that NOHA displaces the metal-bridging hydroxide ion (*23*, *54*−*55*). The hydroxyl oxygen resides deeper in the active-site cleft in a location 1.7 Å away from that of the metal-bridging hydroxide ion in the native enzyme. Additionally, the Mn^{2+}_A−Mn^{2+}_B separation increases from 3.3 Å in the native enzyme (*35*) to 3.9 Å in the NOHA complex. Due to the close proximity of the NOHA hydroxyl oxygen to direct metal ligands Asp-232 and Asp-234, these side chains move slightly relative to the native enzyme and Asp-232 weakens its coordination interaction to the outer sphere of Mn^{2+}_A (Oδ2···Mn^{2+}_A separation = 3.1 Å). If the outer-sphere interaction between the NOHA hydroxyl oxygen···Mn^{2+}_A is considered, then the coordination geometry of Mn^{2+}_A is distorted tetrahedral: Asp-124, His-101, Asp-128, and the hydroxyl oxygen of NOHA coordinate to Mn^{2+}_A. The metal coordination geometry of Mn^{2+}_B remains distorted octahedral.

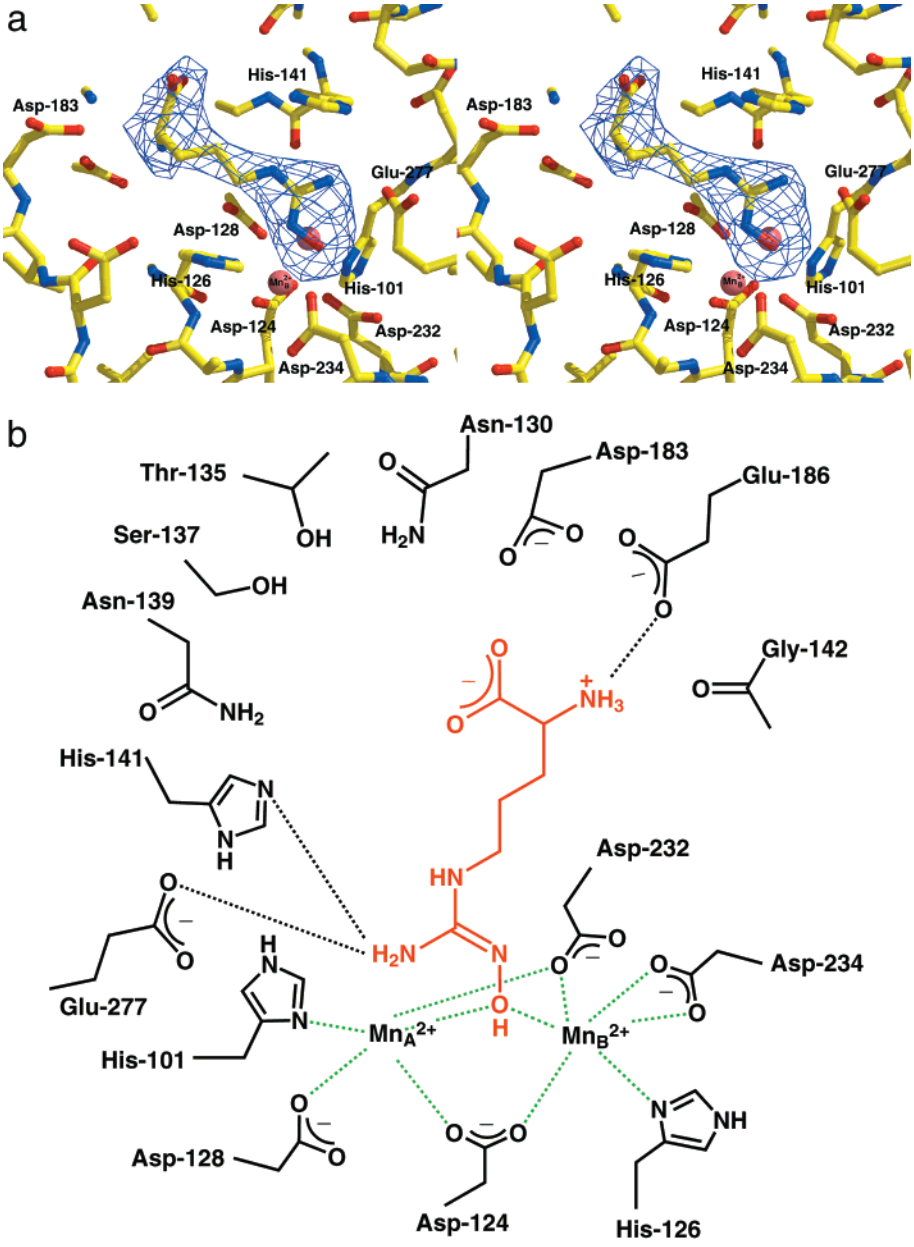

FIGURE 4: Arginase−NOHA complex. (a) Omit electron density map of NOHA in the arginase active site calculated with SIGMAA-weighted (*79*) coefficients $|F_o| - |F_c|$ averaged over the three monomers in the asymmetric unit. The map is contoured at 4σ and selected active-site residues are indicated. Atoms are color-coded as follows: C = yellow, O = red, N = blue; water molecules appear as red spheres. (b) Summary of intermolecular interactions. Manganese coordination interactions are designated by green dashed lines, and hydrogen bonds are indicated by black dashed lines.

The η-NH_2 group of NOHA donates a hydrogen bond to Glu-277 (N···Oϵ2 separation = 2.5 Å) and the side chain of His-141 (N···Nδ1 separation = 2.9 Å). This is consistent with the role of substrate binding proposed for Glu-277 upon inspection of the structure of native arginase (*35*). Additionally, this is consistent with the role of His-141 in substrate binding implicated in the site-directed mutagenesis experiments of Cavalli and colleagues, in which His-141 → Asn arginase exhibits 6-fold increased K_M values (*42*). Finally, the ϵ-NH group of NOHA is in close proximity to Nϵ2 of His-141, with ϵ-NH···Nϵ2 separation = 3.1 Å.

The α-carboxylate of NOHA makes no hydrogen bond interactions with the protein and the α-amino nitrogen makes a single hydrogen bond with Glu-186 (N···Oϵ2 separation = 3.2 Å). We cannot rule out the possibility of water-bridged hydrogen bonds between the α-substituents of NOHA and active-site residues: at the modest resolution of the crystal structure determination, not all such water molecules are expected to be observable. Even so, the relative dearth of interactions between α-substituents of NOHA and arginase is in stark contrast to the binding of other amino acids such as ABH (*7*), BEC (*38*), and L-ornithine (this work). The bulky, rigid nature of the NOHA hydroxyguanidino group may restrict the α-substituents from achieving an optimal constellation of hydrogen bond interactions in the arginase active site, and this may account for the relatively modest binding affinity with $K_i = 10-42$ μM (*9*, *23*). It is interesting that the IC_{50} value of descarboxy−NOHA toward arginase is 50 times higher than that of NOHA (Table 1). This indicates that the α-carboxylate group of NOHA plays an important role in the binding of NOHA to arginase, despite the lack of hydrogen bond interactions deduced from the

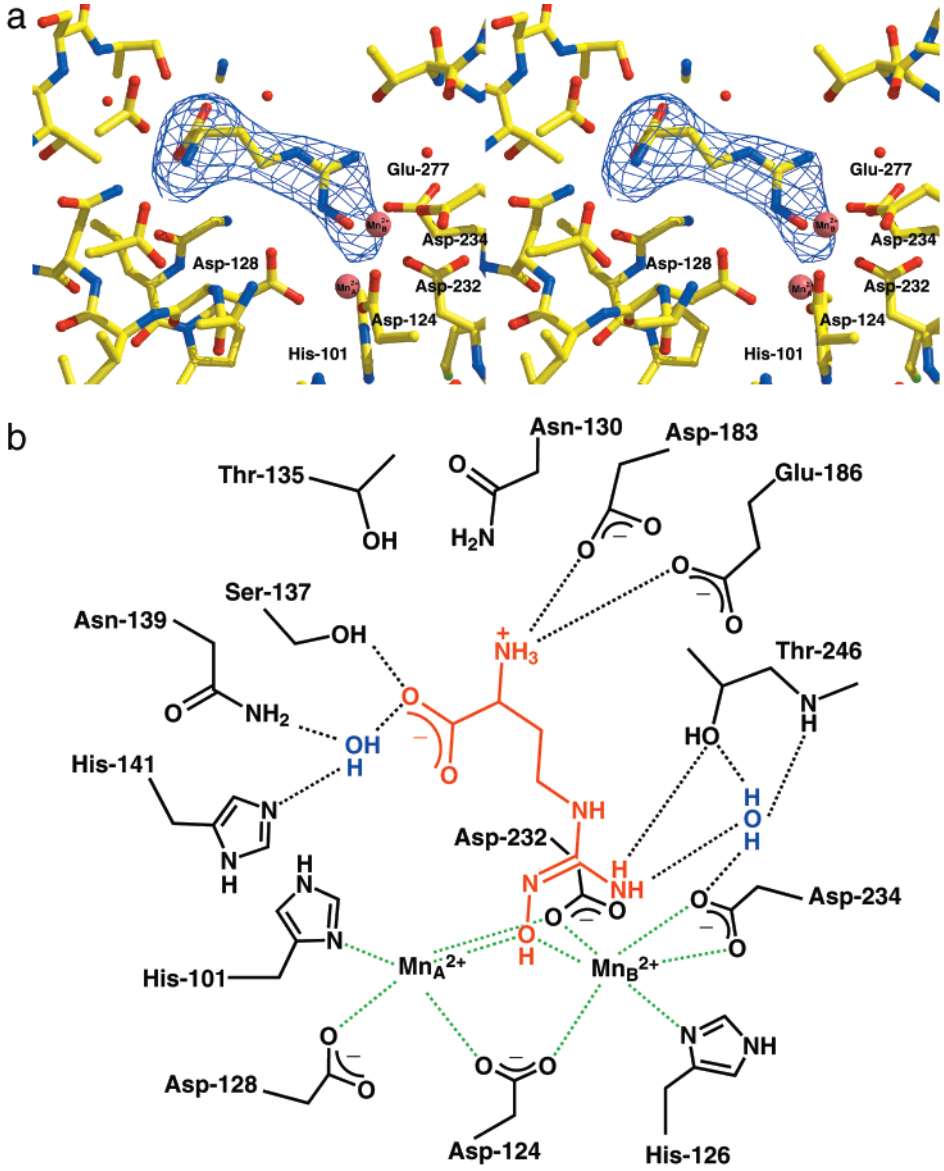

FIGURE 5: Arginase−*nor*-NOHA complex. (a) Omit electron density map of *nor*-NOHA in the arginase active site calculated with SIGMAA-weighted (*79*) coefficients $|F_o| - |F_c|$ averaged over the three monomers in the asymmetric unit. The map is contoured at 4σ and selected active-site residues are indicated. Atoms are color-coded as follows: C = yellow, O = red, N = blue; water molecules appear as red spheres. The orientation is rotated ~90° in the plane of the page relative to Figure 4 for clarity. (b) Summary of intermolecular interactions. Manganese coordination interactions are designated by green dashed lines, and hydrogen bonds are indicated by black dashed lines.

crystal structure. Possibly, the α-carboxylate group engages in a water-bridged hydrogen bond with the active site, but the bridging water molecule is not observed due to the modest resolution of the crystal structure determination. Observed intermolecular interactions are summarized in Figure 4b.

Wild-Type Arginase−nor-NOHA Complex. No major changes are observed in the overall structure of the arginase−*nor*-NOHA complex relative to native arginase; the rms deviation of 314 Cα atoms between the two structures is 0.34 Å. The average thermal B factors of the protein and *nor*-NOHA are 87 and 86 Å^2, respectively. The omit map of Figure 5a reveals that the hydroxyl oxygen of *nor*-NOHA displaces the metal-bridging hydroxide ion of the native enzyme (*35*) and asymmetrically bridges $Mn^{2+}{}_A$ and $Mn^{2+}{}_B$ with oxygen−metal separations of 2.5 and 2.6 Å, respectively. The hydroxyl oxygen of *nor*-NOHA is located 0.8 Å from the position of the metal-bridging hydroxide ion in the native structure. Upon binding *nor*-NOHA, Asp-232 moves by about 0.35 Å to an outer-sphere coordination interaction with $Mn^{2+}{}_A$ (Oδ2···$Mn^{2+}{}_A$ separation = 2.7 Å). The $Mn^{2+}{}_A$−$Mn^{2+}{}_B$ separation increases to 3.5 Å. These observations are in agreement with electron paramagnetic resonance studies of the arginase−*nor*-NOHA complex, which indicated that the hydroxyl group of *nor*-NOHA displaces the metal-bridging hydroxide (*23*).

The ζ-NH_2 group of *nor*-NOHA donates a hydrogen bond to the side-chain hydroxyl group of Thr-246 (2.6 Å) and water 607. Water 607 hydrogen bonds to the carboxylate side chain of Asp-234 and the side-chain oxygen and backbone nitrogen atoms of Thr-246 (both 2.9 Å). Finally, the α-amino acid moiety of *nor*-NOHA makes an array of interactions (Figure 5b), many of which are observed in the binding of ABH (*7*), BEC (*38*), and L-ornithine (Figure 2b). Compared with NOHA, the removal of a side-chain methylene group in *nor*-NOHA allows the α-carboxylate and α-amino groups to engage in several additional hydrogen bond interactions. These structural features likely account

for the increased affinity of *nor*-NOHA [$K_i = 0.5$ μM (*23*)] relative to NOHA [$K_i = 10-42$ μM (*9*, *23*)]. A comparison of the IC_{50} values of *nor*-NOHA and its descarboxy and des-(α-amino) analogues toward arginase (Table 1) shows a more dramatic decrease in the affinity of *nor*-NOHA after deletion of the α-amino group than after deletion of the α-carboxylate group. This suggests that the charge−charge interactions of the α-amino group with Asp-183 and Glu-186 provide greater stabilization than the charge-dipole interactions of the α-carboxylate group with Ser-137, Asn-130, and Thr-135 via a bridging water molecule (Figure 5b).

DISCUSSION

The structures reported herein, when interpreted in view of enzymological data as well as other recently determined arginase structures, provide an unparalleled view of structure-mechanism relationships for arginase. The structure-based mechanism is discussed below and summarized in Figure 6.

Substrate Binding. Modeling studies accompanying the structure determination of the native enzyme (*35*) suggest that the substrate guanidinium group can salt link with Glu-277, which would position the scissile guanidinium carbon directly in-line with the metal-bridging hydroxide ion for nucleophilic attack. Accordingly, a metal-activated hydroxide mechanism is favored for L-arginine hydrolysis, and the pK_a of 7.9 in the pH-rate profile may correspond to the ionization that yields the nucleophilic metal-bridging hydroxide ion (*56*). There is ample precedent for nucleophilic metal-bridging hydroxide ions in other hydrolytic metalloenzymes (*57*−*60*) as well as examples found in biomimetic systems (*61*−*65*).

X-ray crystallographic studies of the *B. caldovelox* arginase−L-arginine complex inactivated by depletion of $Mn^{2+}{}_B$ partially support this proposal: η_1-NH_2 of L-arginine donates hydrogen bonds to Oϵ2 of Glu-277 (Glu-271 in *B. caldovelox* arginase) and the backbone carbonyl of His-141 (His-139 in *B. caldovelox* arginase), and η_2-NH_2 donates hydrogen bonds to the hydroxyl side chain of Thr-246 (Thr-240 in *B. caldovelox* arginase) and a metal-bound solvent molecule (*66*). In the current study, the η-NH_2 group of the substrate analogue NOHA donates hydrogen bonds to Glu-277 and the side chain of His-141. In the arginase−*nor*-NOHA complex, Thr-246 accepts a hydrogen bond from the ζ-NH_2 group of the inhibitor. Only the hydroxyl groups of NOHA and *nor*-NOHA coordinate to Mn^{2+}, so a metal coordination interaction is unlikely for the substrate L-arginine, which of course lacks a hydroxyl group. Since K_M values do not vary significantly among His-141 variants (*42*, *67*), it is the main-chain carbonyl oxygen of His-141 that makes the more important interaction with an actual substrate. Therefore, we conclude that Glu-277, Thr-246, and the backbone carbonyl of His-141 are critical for substrate binding and alignment of the guanidinium group in the first step of the arginase mechanism.

Enzymological and structural data argue against a direct substrate guanidine−metal coordination interaction in the precatalytic Michaelis complex: the substrate K_M value (which reflects enzyme−substrate affinity) does not change significantly when the binuclear manganese cluster is perturbed by site-directed mutagenesis (*42*), nor does it change when $Mn^{2+}{}_A$ is dialyzed out of the active site (*42*, *68*). This is consistent with the three-dimensional active-site contour, which is sterically constricted such that nucleophilic attack of metal-bound hydroxide (bridging or terminal) at a putative metal-bound guanidinium group is geometrically hindered.

Despite these arguments, structural studies of $Mn^{2+}{}_B$-depleted *B. caldovelox* arginase complexed with L-arginine are interpreted to reveal a long-range coordination interaction between the η_1-NH_2 of the substrate and $Mn^{2+}{}_A$ ($N\cdots Mn^{2+}{}_A$ separation = 2.52 Å) (*66*). Baker and colleagues argue that the bond angles of this nitrogen with $Mn^{2+}{}_A$ and hydrogen-bonding partners are consistent with sp^3 hybridization, therefore implying that unprotonated L-arginine binds to arginase. As proposed by Dismukes (*54*), L-arginine could be deprotonated by His-141 prior to metal coordination. However, this mechanistic alternative does not explain the ∼10% residual activity measure for His-141 → Asn arginase (*42*); furthermore, mechanistic proposals that invoke a precatalytic guanidine-metal interaction (*54*, *66*) must proceed through an unusual tetrahedral intermediate bearing a negative charge on an electropositive nitrogen atom. It is clear that unprotonated L-arginine from solution is not the substrate, which would require an exceptionally low K_M value of $\sim 10^{-9}$ M at physiological pH. With $k_{cat} = 250$ s^{-1}, this would yield $k_{cat}/K_M = 2.5 \times 10^{11}$ M^{-1} s^{-1}, clearly violating the limit of diffusion control.

Transition State/Tetrahedral Intermediate Binding. Nucleophilic attack of the metal-bridging hydroxide ion at substrate L-arginine aligned by Glu-277 and His-141 results in a neutral tetrahedral intermediate (Figure 6). The tight binding of tetrahedral transition-state analogue inhibitors is consistent with such an intermediate in catalysis. Among the tightest-binding arginase inhibitors are the boronic acid analogues of L-arginine, ABH and BEC ($K_d = 0.11$ μM and $K_d = 2.22$ μM, respectively) (*36*−*38*). Although designed and synthesized as trigonal planar isosteres of the substrate, both ABH and BEC bind to arginase as the tetrahedral boronate anions (*7*, *38*). The metal-bridging hydroxide ion may attack the trigonal planar boronic acid to yield the tetrahedral boronate anion, thereby mimicking the nucleophilic attack of metal-bridging hydroxide ion at the trigonal planar guanidinium group of the substrate in catalysis.

Both ABH and BEC bind with one boronate hydroxyl group symmetrically bridging the binuclear manganese cluster and donating a hydrogen bond to Asp-128. A second boronate hydroxyl group engages in a coordination interaction with the open coordination site on $Mn^{2+}{}_A$ and also donates a hydrogen bond to the backbone carbonyl of His-141. Upon binding the transition-state inhibitors, $Mn^{2+}{}_A$ undergoes a change in coordination geometry from square pyramidal in the native enzyme to distorted octahedral in the enzyme−inhibitor complex. The coordination geometry of $Mn^{2+}{}_B$ remains distorted octahedral. The interactions observed in these arginase complexes yield important insight on the transition-state stabilization afforded by the arginase active site. The binuclear manganese cluster of arginase not only activates metal-bridging hydroxide, but it also stabilizes the corresponding hydroxyl group in the tetrahedral intermediate. Additionally, $Mn^{2+}{}_A$ stabilizes the transition state by coordinating the lone electron pair that develops on the terminal amino group of the tetrahedral intermediate. Notably, this interaction is specific for the transition state and

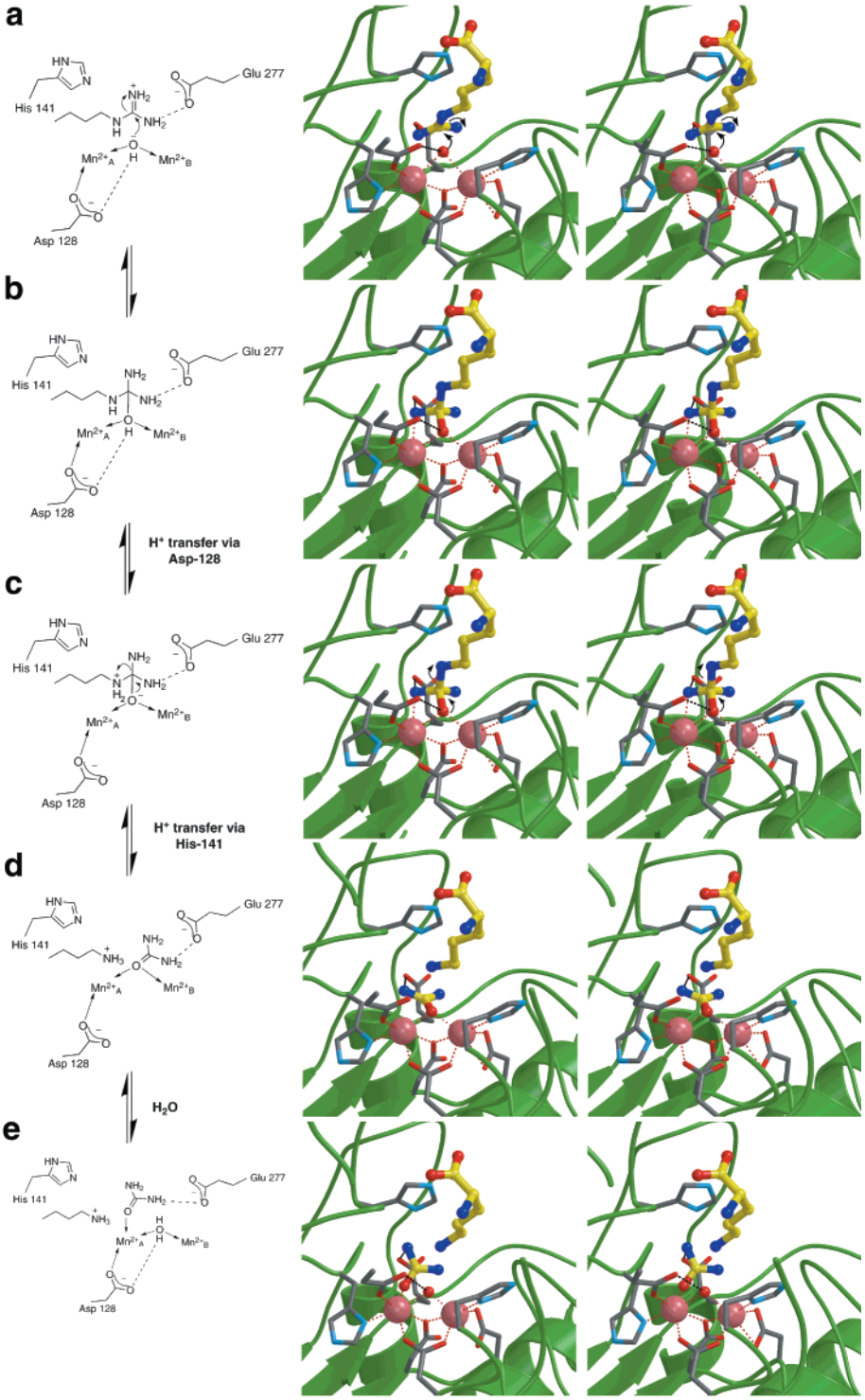

FIGURE 6: Structure-based arginase mechanism. (Left) Schematic representation of the arginase mechanism clarified by structural inferences emanating from the current study; α-amino and α-carboxylate substrate groups are omitted for clarity. (Middle, right) Stereoview of the arginase mechanism. Protein atoms are color-coded as follows: C = gray, O = red, N = blue; ligand atoms are color-coded the same with the exception: C = yellow; water molecules appear as red spheres. Manganese coordination interactions are designated by red dashed lines, and hydrogen bonds by black dashed lines. (a) Binding of the substrate L-arginine to arginase; the substrate guanidium group does *not* coordinate to the manganese ions. Model constructed manually and based on structures of inactive *B. caldovelox* arginase−L-arginine complex (*66*), rat liver arginase−NOHA and arginase−*nor*-NOHA complexes (this work), and analysis of native arginase structure (*35*). (b) Nucleophilic attack of metal-bridging hydroxide at the substrate guanidinium group leads to formation of a tetrahedral intermediate. Model constructed manually and based on arginase-ABH and arginase-BEC complexes (*7*, *38*). (c, d) Following a proton transfer to the leaving amino group mediated by Asp-128—which is consistent with binding conformations of tetrahedral transition-state analogues ABH and BEC (*7*, *38*)—the collapse of the tetrahedral intermediate yields products L-ornithine and urea. Model constructed manually and based on analysis of native enzyme structure (*35*). (e) A water molecule enters to bridge the binuclear Mn^{2+} cluster, causing the urea product to move to a terminal coordination site on Mn^{2+}_A; product dissociation facilitates ionization of the metal-bridging water molecule to yield the catalytically active hydroxide ion. Proton transfer from metal-bridging water to bulk-solvent is mediated by the side chain of His-141. Possibly, the product L-ornithine could abstract a proton from metal-bridging water prior to product dissociation, but this would not account for the catalytic importance of His-141 (*42*, *67*−*68*). Model shows the structure of the arginase−L-ornithine−urea complex (this work).

tetrahedral intermediate *only*: this interaction cannot be achieved by the substrate because the nitrogen lone electron pair is delocalized in the guanidinium π system.

Product Binding. Upon proton transfer to the leaving amino group of ornithine mediated by Asp-128, the final tetrahedral intermediate collapses to yield products L-ornithine and urea (Figure 6). As demonstrated in site-directed mutagenesis and chemical labeling experiments (*42*, *67*), His-141 is a catalytically important residue and may play a role in catalysis as a proton shuttle. The side chain of His-141 may shuttle a proton from bulk solvent to the ϵ-amino group of L-ornithine before product dissociation in the hydrolysis reaction. This is consistent with the structure of the H141C arginase-products complex, in which the ϵ-NH_3^+ group of L-ornithine is ∼3 Å from the former position of the His-141 side chain in the wild-type enzyme.

Notably, His-141 may facilitate the ionization of a metal-bridging water molecule by shuttling the dissociated proton to bulk solvent, thereby regenerating the nucleophilic metal-bridging hydroxide ion. Such a role is analogous to the proton shuttle role of His-64 in the zinc metalloenzyme carbonic anhydrase II (*69*−*71*). In arginase, this important catalytic step may be hindered by the His-141 → Cys mutation, which may account for the diminished k_{cat} measured for this variant.

The structure of the H141C arginase−L-ornithine−urea complex reveals that the hydrogen bond initially formed between the η_1-NH_2 group of substrate L-arginine and Glu-277 prior to catalysis is preserved upon product urea formation. However, collapse of the tetrahedral intermediate returns the nitrogen lone electron pair into the delocalized π system of urea, thereby disrupting the amino-Mn^{2+}_A coordination interaction that stabilized the preceding tetrahedral intermediate and its flanking transition states. However, the urea oxygen, which derives from the metal-bridging hydroxyl group of the preceding tetrahedral intermediate, moves to a terminal coordination site on Mn^{2+}_A in order to facilitate the binding of a metal-bridging solvent molecule. Accordingly, the release of products L-ornithine and urea can occur *after* the binding of the water molecule that regenerates the catalytic nucleophile, metal-bridging hydroxide. Since the arginase reaction is characterized as a uni-bi reaction with a rapid equilibrium-random mechanism, there is no preferential order of product release from the arginase−L-ornithine−urea complex (*39*).

CONCLUDING REMARKS AND METABOLIC INFERENCES

The structural data presented in this paper interpreted in light of previous enzymological and structural data are consistent with a metal-activated hydroxide mechanism for catalysis by arginase. The structure-based mechanism is summarized in Figure 6. The electrophilic carbon of the substrate is oriented in-line with the metal-bridging hydroxide ion by hydrogen bonds with Glu-277, Thr-246, and the backbone carbonyl of His-141. The tetrahedral intermediate and its flanking transition states are stabilized by bridging and terminal metal coordination interactions with the binuclear manganese cluster. Product release is facilitated by the binding of water to the metal cluster to regenerate the nucleophilic metal-bridging hydroxide ion.

Additionally, the arginase−NOHA complex provides the first structural mechanistic link between arginase and NO synthase. The molecular recognition of NOHA contrasts between arginase and NO synthase (*30*, *31*, *44*) (Figure 7). X-ray crystal structures of the NO synthase−NOHA complex (*30*, *31*) reveal numerous hydrogen bond interactions. Specifically, Glu-371 (NO synthase II sequence) accepts hydrogen bonds from the side-chain ϵ-NH and η-NH_2 groups of NOHA, and the η-NH_2 group of NOHA donates a hydrogen bond to the backbone carbonyl of Trp-366. These interactions position the hydroxyguanidinium moiety above the active-site heme group. However, NOHA does not coordinate to the heme iron. The backbone NH group of Gly-365 donates a hydrogen bond to the NOHA hydroxyl group, which may contribute to the slight (8−10°) distortion from planarity. This contrasts with hydroxyguanidinium interactions in the arginase−NOHA complex, where the metal coordination interaction by the hydroxyl group dominates NOHA recognition (Figures 4 and 7). Although no deformation of the NOHA hydroxyguanidinium group is apparent in the arginase−NOHA complex, it is notable that two hydroxyguanidinium structures retrieved from the CSD exhibit ∼7−14° hydroxyl deformations (*72*−*73*).

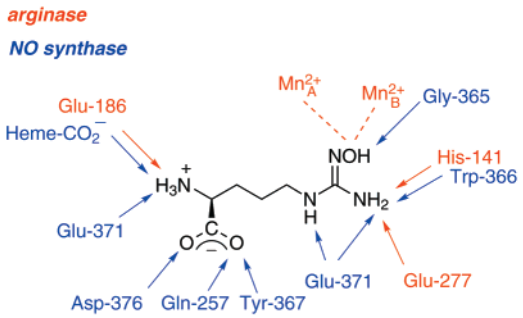

FIGURE 7: Scheme contrasting the molecular recognition of NOHA by arginase and NO synthase. Arginase−NOHA interactions are labeled in red: manganese coordination interactions are designated by red dashed lines, and hydrogen bonds are indicated by red arrows. NO synthase−NOHA hydrogen bond interactions are designated by blue arrows.

The α-amino and α-carboxylate moieties of NOHA make numerous interactions in the active-site channel of NO synthase (*30*−*31*), including hydrogen bonds with Tyr-367, Asp-376, Gln-257, Glu-371, and a heme carboxylate. This contrasts with recognition of the NOHA α-substituents by arginase, which engages in only a single hydrogen bond with the α-amino group of NOHA (Figures 4 and 7).

The inhibition of arginase by NOHA, the key intermediate in NO biosynthesis, reflects a potential metabolic relationship between NO synthase and arginase. The concentration of NOHA in human plasma is about 9 μM (*74*) and rises to 37 μM in lipopolysaccharide-treated rats due to elevated levels of inducible NO synthase (*25*). These NOHA concentrations are sufficient to cause appreciable arginase inhibition (*24*−*25*, *74*): for example, 100 μM NOHA in endothelial cells causes a 2-fold reduction in urea production (*24*). The effective concentration of NOHA required for arginase inhibition is probably lower than 100 μM due to the relatively short half-life of NOHA (24 h) (*24*) and the fact that NOHA is a substrate for other enzymes in addition to NO synthase, including peroxidases, cytochromes P-450, hemoglobin, and catalase (*75*−*76*). Therefore, the observed arginase inhibition is consistent with the K_i for NOHA of 10−42 μM (*9*, *23*). Since arginase can regulate NO synthase by depleting the

substrate pool of L-arginine available for NO biosynthesis, as discussed in the preceding paper in this issue by Kim and colleagues (*38*), the reciprocal relationship between these two enzymes is manifest not only at the level of transcriptional regulation (*8*, *12*−*16*, *77*−*78*) but also at the level of catalytic activity. Another facet of this reciprocal catalytic relationship is now evident in the contrasting molecular recognition of NOHA by arginase and NO synthase.

ACKNOWLEDGMENT

We thank Drs. Ron Viola and Michael Rynkiewicz for helpful discussions and Kevin Compher for assistance with crystal growth. Diffraction data for the H141C arginase−L-ornithine−urea complex and the arginase−NOHA complex were collected at beamline 7-1 at the Stanford Synchrotron Radiation Laboratory, which is funded by the Department of Energy and the National Institutes of Health. Data for the arginase−*nor*-NOHA complex were collected at beamline 17-ID in the facilities of the Industrial Macromolecular Crystallography Association-Collaborative Access Team at the Advanced Photon Source. These facilities are supported by the companies of the Industrial Macromolecular Crystallography Association through a contract with the Center for Synchrotron Radiation Research and Instrumentation at the Illinois Institute of Technology. The Advanced Photon Source is supported by the U.S. Department of Energy.

REFERENCES

1. Wu, G., and Morris, S. M., Jr. (1998) *Biochem. J. 336*, 1−17.
2. Iyer, R., Jenkinson, C. P., Vockley, J. G., Kern, R. M., Grody, W. W., and Cederbaum, S. (1998) *J. Inherited Metab. Dis. 21* (Suppl. 1), 86−100.
3. Christianson, D. W., and Cox, J. D. (1999) *Annu. Rev. Biochem. 68*, 33−57.
4. Ash, D. E., Cox, J. D., and Christianson, D. W. (2000) in Manganese and its Role in Biological Processes. In *Metal Ions in Biological Systems* (Sigel A., and Sigel, H., Eds.) Vol. 37, pp 408−428, Marcel Dekker, New York.
5. Herzfeld, A., and Raper, S. M. (1976) *Biochem. J. 153*, 469−478.
6. Baggio, R., Emig, F. A., Christianson, D. W., Ash, D. E., Chakder, S., and Rattan, S. J. (1999) *Pharmacol. Exp. Ther. 290*, 1409−1416.
7. Cox, J. D., Kim, N. N., Traish., A. M., and Christianson, D. W. (1999) *Nat. Struct. Biol. 6*, 1043−1047.
8. Corraliza, I. M., Soler, G., Eichmann, K., and Modolell, M. (1995) *Biochem. Biophys. Res. Commun. 206*, 667−673.
9. Daghigh, F., Fukuto, J. M., and Ash, D. E. (1994) *Biochem. Biophys. Res. Commun. 202*, 174−180.
10. Chenais, B., Yapo, A., Lepoivre, M., and Tenu, J.-P. (1993) *Biochem. Biophys. Res. Commun. 196*, 1558−1565.
11. Klatt, P., Schmidt, K., Uray, G., and Mayer, B. J. (1993) *J. Biol. Chem. 268*, 14781−14787.
12. Keller, R., Gehri, R., Keist, R., Huf, E., and Kayser, F. H. (1991) *Cell. Immunol. 134*, 249−256.
13. Albina, J. E., Henry, W. L., Mastrofrancesco, B., Martin, B.-A., and Reichner, J. S. (1995) *J. Immunol. 155*, 4391−4396.
14. Albina, J. E., Mills, C. D., Henry, W. L., and Caldwell, M. D. (1990) *J. Immunol. 144*, 3877−3880.
15. Wang, W. W., Jenkinson, C. P., Griscavage, J. M., Kern, R. M., Arabolos, N. S., Byrns, R. E., Cederbaum, S. D., and Ignarro, L. J. (1995) *Biochem. Biophys. Res. Commun. 210*, 1009−1016.
16. Gotoh, T., Sonoki, T., Nagasaki, A., Terada, K., Takiguchi, M., and Mori, M. (1996) *FEBS Lett. 395*, 119−122.
17. Morris, S. M., Jr., Bhamidipati, D., and Kepka-Lenhart, D. (1997) *Gene 193*, 157−161.
18. Pufahl, R. A., Nanjappan, P. G., Woodard, R. W., and Marletta, M. A. (1992) *Biochemistry 31*, 6822−6828.
19. Stuehr, D. J., Kwon, N. S., Nathan, C. F., Griffith, O. W., Feldman, P. L., and Wiseman, J. (1991) *J. Biol. Chem. 266*, 6259−6263.
20. Kerwin, J. F., Lancaster, J. R., and Feldman, P. L. (1995) *J. Med. Chem. 38*, 4343−4362.
21. Masters, B. S. S., McMillan, K., Sheta, E. A., Nishimura, J. S., Roman, L. J., and Martasek, P. (1996) *FASEB J. 10*, 552−558.
22. Pfeiffer, S., Mayer, B., and Hemmens, B. (1999) *Angew. Chem., Int. Ed. Engl. 38*, 1714−1731.
23. Custot, J., Moali, C., Brollo, M., Boucher, J.-L., Delaforge, M., Mansuy, D., Tenu, J. P., and Zimmermann, J. L. (1997) *J. Am. Chem. Soc. 119*, 4086−4087.
24. Buga, G. M., Singh, R., Pervin, S., Rogers, N. E., Schmitz, D. A., Jenkinson, C. P., Cederbaum, S. D., and Ignarro, L. J. (1996) *Am. J. Physiol. 271*, H1988−H1998.
25. Hecker, M., Nematollahi, H., Hey, C., Busse, R., and Racke, K. (1995) *FEBS Lett. 359*, 251−254.
26. Moali, C., Boucher, J.-L., Sari, M.-A., Stuehr, D. J., and Mansuy, D., (1998) *Biochemisty 37*, 10453−10460.
27. Rogriguez-Crespo, I., Gerber, N. C., and Ortiz de Montellano, P. R. (1996) *J. Biol. Chem. 271*, 11462−11467.
28. Klatt, P., Schmidt, K., Uray, G., and Mayer, B. (1993) *J. Biol. Chem. 268*, 14781−14787.
29. Ghosh, D. K., Abu-Soud, H. M., and Stuehr, D. J. (1995) *Biochemistry 34*, 11316−11320.
30. Crane, B. R., Arvai, A. S., Ghosh, S., Getzoff, E. D., Stuehr, D. J., and Tainer, J. A. (2000) *Biochemistry 39*, 4608−4621.
31. Fischmann, T. O., Hruza, A., Niu, X. D., Fossetta, J. D., Lunn, C. A., Dolphin, E., Prongay, A. J., Reichert, P., Lundell, D. J., Narula, S. K., and Weber, P. C. (1999) *Nat. Struct. Biol. 6*, 233−242.
32. Raman, C. S., Li, H., and Poulos, T. L. (2001) Personal communication cited in Tierney, D. L., Huang, H., Martasek, P., Masters, B. S. S., Silverman, R. B., and Hoffman, B. M. (1999) *Biochemistry 38*, 3704−3710.
33. Custot, J., Boucher, J.-L., Vadon, S., Guedes, C., Dijols, S., Delaforge, M., and Mansuy, D. (1996) *J. Biol. Inorg. Chem. 1*, 73−82.
34. Vadon, S., Custot, J., Boucher, J.-L., and Mansuy, D. (1996) *J. Chem. Soc., Perkin Trans. 1*, 645−648.
35. Kanyo, Z. F., Scolnick, L. R., Ash, D. E., and Christianson, D. W. (1996) *Nature 383*, 554−557.
36. Baggio, R., Elbaum, D., Kanyo, Z. F., Carroll, P. J., Cavalli, R. C., Ash, D. E., and Christianson, D. W. (1997) *J. Am. Chem. Soc. 119*, 8107−8108.
37. Baggio, R., Cox, J. D., Harper, S. L., Speicher, D. W., and Christianson, D. W., (1999) *Anal. Biochem. 276*, 251−253.
38. Kim, N. N., Cox, J. D., Baggio, R. F., Emig, F. A., Mistry, S., Harper, S. L., Speicher, D. W., Morris, S. M., Ash, D. E., Traish, A. M., and Christianson, D. W. (2001) *Biochemistry 40*, 2678−2688.
39. Reczkowski, R. S., and Ash, D. E. (1994) *Arch. Biochem. Biophys. 312*, 31−37.
40. Fuentes, J. M., Campo, M. L., and Soler, G. (1994) *Arch. Int. Physiol. Biochim. Biophys. 102*, 255−258.
41. Carvajal, N., and Cederbaum, S. D. (1986) *Biochim. Biophys. Acta 870*, 181−184.
42. Cavalli, R. C., Burke, C. J., Kawamoto, S., Soprano, D. R., and Ash, D. E. (1994) *Biochemistry 33*, 10652−10657.
43. Higuchi, R., Krummel, B., and Saiki, R. K. (1988) *Nucleic Acids Res. 16*, 7351−7367.
44. Moali, C., Brollo, M., Custot, J., Sari, M.-A., Boucher, J.-L., Stuehr, D. J., and Mansuy, D. (2000) *Biochemistry 39*, 8208−8218.
45. Kanyo, Z. F., Chen, C. Y., Daghigh, F., Ash, D. E., and Christianson, D. W. (1992) *J. Mol Biol. 224*, 1175−1177.
46. Otwinowski, Z., and Minor, W. (1997) *Methods Enzymol. 276*, 307−326.
47. Navaza, J. (1994) *Acta Crystallogr., Sect. A 50*, 157−163.
48. Collaborative Computational Project, Number 4. (1994) *Acta Crystallogr., Sect. D 50*, 760−763.

49. Brünger, A. T., Adams, P. D., Clore, G. M., DeLano, W. L., Gros, P., Grosse-Kunstleve, R. W., Jiang, J. S., Kuszewski, J., Nilges, M., Pannu, N. S., Read, R. J., Rice, L. M., Simonson, T., and Warren, G. L. (1998) *Acta Crystallogr., Sect. D 54*, 905−921.
50. Jones, T. A., Zou, J.-Y., Cowan, S. W., and Kjeldgaard, M. (1991) *Acta Crystallogr., Sect. A 47*, 110−119.
51. Esnouf, R. M. (1997) *J. Mol. Graphics 15*, 132−134.
52. Merritt, E. A., and Bacon, D. J. *Methods Enzymol. 277*, 505−524 (1997).
53. Allen, F. H., Kennard, O., Taylor, R. (1983) *Acc. Chem. Res. 16*, 146−153.
54. Khangulov, S. V., Sossong, T. M., Jr., Ash, D. E., and Dismukes, G. C. (1998) *Biochemistry 37*, 8539−8550.
55. Sossong, T. M., Khangulov, S. V., Cavalli, R. C., Soprano, D. R., Dismukes, G. C., and Ash, D. E. (1997) *J. Biol. Inorg. Chem. 2*, 433−443.
56. Kuhn, N. J., Talbot, J., and Ward, S. (1991) *Arch. Biochem. Biophys. 286*, 217−221.
57. Heikinheimo, P., Lehtonen, J., Baykov, A., Lahti, R., Cooperman, B. S., and Goldman, A. (1996) *Structure 4*, 1491−1508.
58. Egloff, M. P., Cohen, P. T. W., Reinemer, P., and Barford, D. (1995) *J. Mol. Biol. 254*, 942−959.
59. Wilce, M. C. J., Bond, C. S., Dixon, N. E., Freeman, H. C., Guss, J. M., Lilley, P. E., and Wilce, J. A. (1998) *Proc. Natl. Acad. Sci. U.S.A. 95*, 3472−3477.
60. Sträter, N., and Lipscomb, W. N. (1995) *Biochemistry 34*, 14792−14800.
61. Ye, B. H., Mak, T., Williams, I. D., and Li, X. Y. (1998) *J. Chem. Soc., Dalton Trans*. 1935−1936.
62. Ye, B. H., Mak, T., Williams, I. D., and Li, X. Y. (1997) *Chem. Commun*. 1813−1814.
63. Chapman, W. H., and Breslow, R. (1995) *J. Am. Chem. Soc. 117*, 5462−5469.
64. Williams, N. H., Cheung, W., and Chin, J. (1998) *J. Am. Chem. Soc. 120*, 8079−8087.
65. He, C. H., and Lippard, S. J. (1998) *J. Am. Chem. Soc. 120*, 105−113.
66. Bewley, M. C., Jeffrey, P. D., Patchett, M. L., Kanyo, Z. F., and Baker, E. N. (1999) *Structure 7*, 435−448.
67. Carvajal, N., Olate, J., Salas, M., Uribe, E., López, V., Herera, P., and Cerpa, J. (1999) *Arch. Biochem. Biophys. 371*, 202−206.
68. Scolnick, L. R., Kanyo, Z. F., Cavalli, R. C., Ash, D. E., and Christianson, D. W. (1997) *Biochemistry 36*, 10558−10565.
69. Tu, C. K., Silverman, D. N., Forsman, C., Jonsson, B. H., and Lindskog, S. (1989) *Biochemistry 28*, 7913−7918.
70. Silverman, D. N., and Lindskog, S. (1988) *Acc. Chem. Res. 29*, 30−36.
71. Fierke, C. A., and Christianson, D. W. (1996) *Acc. Chem. Res. 29*, 331−339.
72. Doubell, P. C. J., Oliver, D. W., and van Rooyen, P. H. (1991) *Acta Crystallogr., Sect. C 47*, 353−355.
73. Larsen, I. K. (1975) *Acta Crystallogr., Sect. B 31*, 1626−1629.
74. Meyer, J., Richter, N., and Hecker, M. (1997) *Anal. Biochem. 247*, 11−16.
75. Boucher, J. L., Genet, A., Vadon, S., Delaforge, M., Henry, Y., and Mansuy, D. (1992) *Biochem. Biophys. Res. Commun. 187*, 880−886.
76. Boucher, J. L., Genet, A., Vadon, S., Delaforge, M., and Mansuy, D. (1992) *Biochem. Biophys. Res. Commun. 184*, 1158−1164.
77. Modolell, M., Corraliza, I. M., Link, F., Soler, G., and Eichmann, K. (1995) *Eur. J. Immunol. 25*, 1101−1104.
78. Boutard, V., Havouis, R., Fouqueray, P. C., Moulinoux, J.-P., and Baud, L. (1995) *J. Immunol. 155*, 2077−2084.
79. Read, R. J. (1986) *Acta Crystallogr., Sect. A 42*, 140−149.

BI002318+